TR12 centers in diamond as a room temperature atomic scale vector magnetometer

*Jonas Foglszinger[1], Andrej Denisenko[1], Thomas Kornher[2], Matthias Schreck[3], Wolfgang Knolle[4], Boris Yavkin[5], Roman Kolesov[1], and Jörg Wrachtrup[1]
[1] *3rd Institute of Physics, University of Stuttgart,70569 Stuttgart, Germany*
[2] *Lumiphase AG, Brinerstrasse 21, 8003 Zürich, Switzerland*
[3] *University of Augsburg, Institute of Physics, D-86135 Augsburg, Germany*
[4] *Leibniz Institute for Surface Engineering (IOM), Department Functional Surfaces, D-04318 Leipzig, Germany and*
[5] *Quantronics Group, SPEC, CEA, CNRS, Université Paris-Saclay, 91191 Gif-sur-Yvette CEDEX, France*
(Dated: January 22, 2022)

I. EXPERIMENTAL SETUP

All experiments presented were performed using a home-build confocal microscope (see Fig. S1) working at room temperature. 410 nm laser light is coupled into a single mode polarization maintaining optical fiber to obtain Gaussian mode profile. A polarizing beam splitter (PBS) ensures only one linear polarization is incident on the sample. Combined with the $\lambda/2$-plate right in front of the objective lens, this allows measurements dependent on excitation polarization. The fluorescence light is collected via the same objective lens, split at a dichroic mirror (Wavelengths shorter than 525 nm are reflected while longer wavelengths pass through. This roughly splits the spectrum of TR12 in two equal parts) and detected by two single photon detectors which are based on the principle of avalanche photo diodes (APDs). And additional long pass (450 nm) is added to clear out the remaining laser light before APD 1. The use of two APDS allows for anti-bunching measurement of the fluorescence light.

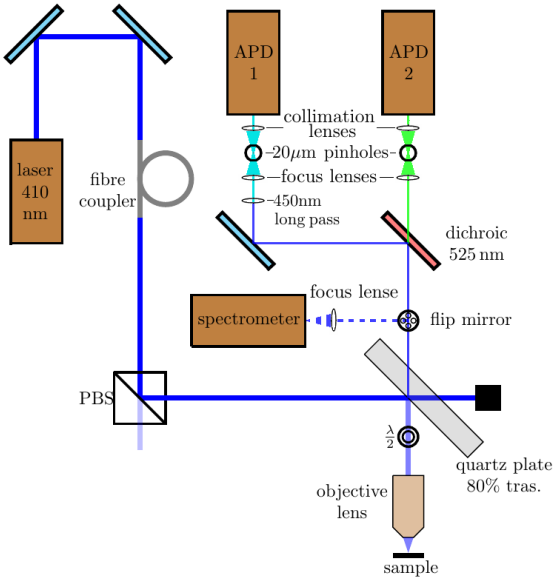

FIG. S1. Schematic representations of the used home-built confocal microscope.

Alternatively, the fluorescence can be deflected to a spectrometer. The collected light is focused through a 20 μm pinhole to ensure a high axial resolution and the confocal nature of the setup.

II. COHERENT POPULATION TRAPPING

This section briefly introduces the basic theory of coherent population trapping (CPT) in a three-level system. The considerations only cover what is needed for the related manuscript. More extended analysis can be found in [1–3], which are based on theoretical foundations such as [4–6].

The observation of CPT, requires a three level system. Its sates are labeled $|T_x\rangle$, $|T_y\rangle$ and $|T_z\rangle$ as in Fig. 1e. The unperturbed Hamiltonian reads

$$\mathrm{H}_0 = \hbar\omega_x |T_x\rangle\langle T_x| + \hbar\omega_y |T_y\rangle\langle T_y| + \hbar\omega_z |T_z\rangle\langle T_z| \ , \quad \text{(S1)}$$

were $\hbar\omega_i$ is the energy for state $|T_i\rangle$. Let $|T_z\rangle$ be the short-lived state while $|T_y\rangle$ and $|T_z\rangle$ are long-lived. If both long-lived states are coupled to the short-lived state via microwaves, this can be expressed as an additional perturbation part in the Hamiltonian

$$\mathrm{H}_1 = -\frac{\hbar}{2}\left(\Omega_p e^{-i\omega_p t}|T_x\rangle\langle T_z| + \Omega_c e^{-i\omega_c t}|T_y\rangle\langle T_z|\right) + \mathrm{H.c}, \quad \text{(S2)}$$

where Ω_p and Ω_c are the two different Rabi frequencies for the transition frequencies $\omega_p = \omega_x - \omega_z$ and $\omega_c = \omega_y - \omega_z$. The Schrödinger equation for the full Hamiltonian $\mathrm{H} = \mathrm{H}_0 + \mathrm{H}_1$ can be solved by applying a general ansatz for the wave functions

$$|\psi(t)\rangle = c_x(t)e^{-i\omega_x t}|T_x\rangle + c_y(t)e^{-i\omega_y t}|T_y\rangle + c_z(t)e^{-i\omega_z t}|T_z\rangle \ . \quad \text{(S3)}$$

The result is a simple set of differential equations for the coefficient functions c_i

$$\begin{aligned} \dot{c_x} &= \frac{i}{2}\Omega_p c_z \\ \dot{c_y} &= \frac{i}{2}\Omega_c c_z \\ \dot{c_z} &= \frac{i}{2}\left(\Omega_p c_x + \Omega_c c_y\right) . \end{aligned} \quad \text{(S4)}$$

It can be easily verified that (S5) is a solution to this system of equations.

$$c_x = \cos(\theta), \quad c_y = -\sin(\theta) \quad \text{and} \quad c_z = 0 \quad \text{where}$$
$$\cos(\theta) = \frac{\Omega_c}{\sqrt{\Omega_c^2 + \Omega_p^2}} \quad \text{and} \quad \sin(\theta) = \frac{\Omega_p}{\sqrt{\Omega_c^2 + \Omega_p^2}}\,. \tag{S5}$$

In other words, there is a dark state $|\psi_D\rangle = \cos(\theta) \cdot |T_x\rangle - \sin(\theta) \cdot |T_y\rangle$, with no probability to be in T_z or change to T_z although T_x and T_y are both coupled to T_z via microwaves. The effect of population being trapped in this dark-state is called coherent population trapping.

The dark state, as superposition, inherits the long lifetime from T_x and T_y. Consequently, it has a rather narrow natural linewidth. In the experiment shown in Fig. 1f, this results in a broad resonance peak with linewidth corresponding mostly to the lifetime of T_z with an additional fluorescence dip with linewidth corresponding to the long lived states T_x and T_y. To complete the argument from the main-text (That the existence of this additional dip confirms the existence of two long lived states T_x and T_y rather than one long lived state T_z), one must realize, that this effect would not occur if the situation was reversed. If the positive contrast in Fig 1.d would result from a long-lived state T_z being coupled to one of the short-lived states T_x or T_y, no such dark state could be formed, as any superposition making all derivatives to zero, would involve at least one short lived state. This superposition would therefore have short lifetime as well and would not allow for any fluorescence quenching with narrow linewidth. The existence of the narrow Fluorescence dip within the broader peak in Fig. 1f therefore indeed confirms the existence of two long lived states T_x and T_y.

III. STEADY STATE SOLUTION

The dynamics in the unperturbed system is simulated using the matrix equation

$$\dot{\rho} = M\rho \tag{S6}$$

with the vector of states
$\rho = (\rho_g(\mathrm{S}_0), \rho_e(\mathrm{S}_1), \rho_x, \rho_y, \rho_z)^{tr}$ and a Matrix

$$M = \begin{pmatrix} -P & \Gamma & \Gamma_X & \Gamma_Y & \Gamma_Z \\ P & -\Gamma - \gamma_x - \gamma_y - \gamma_z & 0 & 0 & 0 \\ 0 & \gamma_x & -\Gamma_X & 0 & 0 \\ 0 & \gamma_y & 0 & -\Gamma_Y & 0 \\ 0 & \gamma_z & 0 & 0 & -\Gamma_Z \end{pmatrix} \tag{S7}$$

defined by the transition rates within the electronic level structure depicted in Fig. 1e. When combining this matrix equation with $\dot{\rho} = 0$ (which equals finding the eigenvector of matrix M to the eigenvalue $EW = 0$ (conservation of population)), the steady state solution can be calculated. As the fluorescence is generated from the transition $\mathrm{S}_1 \rightarrow \mathrm{S}_0$, the fluorescence intensity is directly proportional to the population of the excited state $\rho_e(\mathrm{S}_1)$.

IV. RABI OSCILLATION

In order to simulate the fluorescence during a Rabi oscillation, the equations in S7 are modified to include the respective off-diagonal elements needed. Assuming the coherent driving to take place between the states T_z and T_x, the result reads

$$\begin{aligned}
\dot{\rho_g} &= -P \cdot \rho_g + \Gamma \cdot \rho_e + \Gamma_x \cdot \rho_x + \Gamma_y \cdot \rho_y + \Gamma_z \cdot \rho_z \\
\dot{\rho_e} &= P \cdot \rho_g - (\Gamma + \gamma_x + \gamma_y + \gamma_z) \cdot \rho_e \\
\dot{\rho_x} &= \gamma_x \cdot \rho_e - \Gamma_x \cdot \rho_x + \frac{i\Omega}{2}(\sigma_{zx} - \sigma_{xz}) \\
\dot{\rho_y} &= \gamma_y \cdot \rho_e - \Gamma_y \cdot \rho_y \\
\dot{\rho_z} &= \gamma_z \cdot \rho_e - \Gamma_z \cdot \rho_z + \frac{i\Omega}{2}(\sigma_{xz} - \sigma_{zx}) \\
\dot{\sigma}_{xz} &= \frac{i\Omega}{2}(\rho_z - \rho_x) - \sigma_{xz}\left(\frac{\Gamma_x}{2} + \frac{\Gamma_z}{2}\right) \\
\dot{\sigma}_{zx} &= \frac{i\Omega}{2}(\rho_x - \rho_z) - \sigma_{zx}\left(\frac{\Gamma_x}{2} + \frac{\Gamma_z}{2}\right)\,.
\end{aligned} \tag{S8}$$

For the simulation in Fig. 2c, the system is initialized in the steady state at first using equation (S6) and then evolved with the set of linear differential equations (S8). As the the fluorescence measurement does not take place instantaneously, the system further evolves during this measurement. This is taken into account in the simulation by also further evolving the system for the readout time without Rabi oscillation($\sigma_{xz} = \sigma_{zx} = 0$ in equation (S8)) and averaging the brightness over this interval.

V. NV CENTER AS REFERENCE FOR MAGNETIC MAPS

One major problem of magnetic maps as given in Fig. 2d, is the lack of any reference. While it is obvious that changing the magnet position does change the magnetic field strength and orientation, the exact values can not be read out directly. Also simulating this orientation would not provide a proper solution, as the magnet was centered above the sample rather coarsely which very much reduces the precision of this approach. Instead the process of taking magnetic maps is repeated for NV centers which are known to have their orientation for z aligned with [111] in diamond. In a magnetic map for NV center, this orientation will appear as single bright spot serving as clear reference. When marking the position of this spot in a magnetic map for a TR12 center, a precise reference is given, which reveals the z-orientation of TR12 metastable triplet to be oriented along [111] in diamond

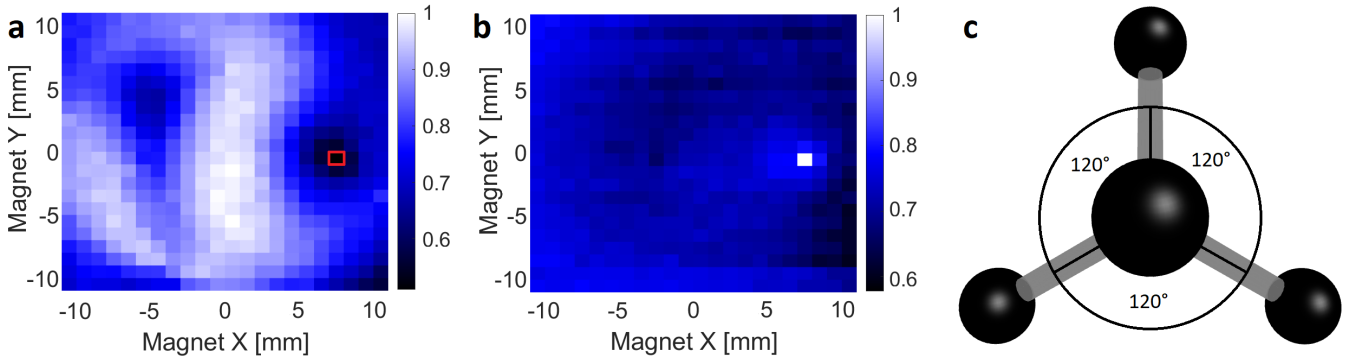

FIG. S2. (a) Measured magnetic map for TR12 center with marked NV z-orientation [111] in diamond. (b) Measured magnetic map for NV center used as a reference for orientation of the magnetic field. (c) Graphic display of the tetrahedron, to illustrate diamond lattice along [111] revealing a threefold symmetry. After rotation by 120° the tetrahedron merges with itself.

as for NV (see Fig. S2a,b) with a maximum deviation of about 5°.

VI. SIMULATING MAGNETIC MAPS AND ORIENTATIONS

As the z-orientation of TR12 metastable triplet is known to be oriented along [111] in diamond, proposing the existence of twelve different orientations is rather straight forward. In diamond lattice there are four distinct orientations for [111] which automatically transfers to four different z-orientations. Imaging the diamond lattice along [111] (See Fig. S2c) a threefold symmetry for rotations around z by 120 ° becomes obvious. Therefore there are three possible orientations for x and y sharing the same z-orientation. This results in twelve inequivalent orientations which are intuitively sorted as four triples.

In order to simulate magnetic maps, the magnetic field in the plane of interest below the magnet is simulated at first. Therefore the permanent magnet is approximated as a cube consisting of uniformly distributed magnetic dipoles. This simulated magnet is then moved virtually above the sample as in the measurement and the resulting magnetic field is calculated at the centers position. As TR12 centers can be oriented differently, the orientation of the magnetic field in the local frame of the center is derived by simple 3d rotations. To simulated the changes in brightness, the effect of this magnetic field on the metastable triplet state is determined.

Without any magnetic field applied, the unperturbed Hamiltonian of the triplet state reads

$$\mathrm{H}_0 = \mathrm{D}(\mathrm{S}_z^2 - S(S+1)/3) + \mathrm{E}(S_x^2 - S_y^2) \tag{S9}$$

with zero-field splitting parameters D and E and the Spin matrices S_x, S_y and S_z for a spin 1 (S=1) system. This Hamiltonian has three eigenvectors $|T_z\rangle = (0,1,0)^{tr}$, $|T_x\rangle = (-1,0,1)^{tr}$ and $|T_y\rangle = (1,0,1)^{tr}$ with eigenvalues $EW_z = -2\mathrm{D}/3$, $EW_x = \mathrm{D}/3 - \mathrm{E}$ and $EW_y = \mathrm{D}/3 + \mathrm{E}$. By defining $EW_i = \hbar\omega_i$ and expressing the Hamiltonian by its eigenvectors, the form in equation (S1) is obtained.

When a static magnetic field is applied in addition, the system Hamiltonian consists of Zero field splitting part (equation (S9)) and Zeeman interaction part $\mathrm{H}_1 = g\mu_B \mathbf{S}\cdot\mathbf{B}$. The total Hamiltonian $\mathrm{H} = \mathrm{H}_0 + \mathrm{H}_1$ then reads

$$\begin{aligned}\mathrm{H} =& \mathrm{D}(\mathrm{S}_z^2 - S(S+1)/3) \\ &+ E(S_x^2 - S_y^2) + g\mu_B \mathbf{S}\cdot\mathbf{B},\end{aligned} \tag{S10}$$

with electron g-factor $g = 2$ and Bohr magneton μ_B. This Hamiltonian again provides three eigenvectors $|\varphi_i\rangle$ which now depend on the magnetic field $\mathbf{B}$. These new eigenvectors can be expressed as linear combinations of the eigenvectors $|T_i\rangle$ resulting from the unperturbed Hamiltonian from equation (S9)

$$|\varphi_i\rangle = \alpha_i \cdot |T_x\rangle + \beta_i \cdot |T_y\rangle + \zeta_i \cdot |T_z\rangle \ , \tag{S11}$$

with mixing coefficients α_i, β_i and ζ_i.

To further proceed the transitions between the ground state - excited state doublet and the unperturbed metastable triplet have to be addressed first. The exact interaction Hamiltonian responsible for the transition from the excited state into the metastable triplet $\mathrm{H}_{\mathrm{int}}^{eT}$ and out of the metastable triplet into the ground state $\mathrm{H}_{\mathrm{int}}^{Tg}$ are unknown. However, the transition rates out of the metastable Triplet $\Gamma_i = |\langle g| H_{\mathrm{int}}^{Tg} |T_i\rangle|^2$ are directly measured and the transition rates into the metastable Triplet $\gamma_i = |\langle e| H_{\mathrm{int}}^{eT} |T_i\rangle|^2$ are calculated in the main text. By assuming that all cross terms average to zero ($\langle g| H_{\mathrm{int}}^{Tg} |T_i\rangle \langle T_j| H_{\mathrm{int}}^{Tg} |g\rangle = \langle e| H_{\mathrm{int}}^{eT} |T_i\rangle \langle T_j| H_{\mathrm{int}}^{eT} |e\rangle = 0$ for $i \neq j$), the new transition rates into (γ_i') and out of (Γ_i') the metastable triplet can be calculated to be

$$\begin{aligned}\gamma_i' =& \left|\langle e| H_{\mathrm{int}}^{eT} |\varphi_i\rangle\right|^2 \\ =& \left|\langle e| H_{\mathrm{int}}^{eT} |\alpha_i \cdot T_x\rangle\right|^2 \\ &+ \left|\langle e| H_{\mathrm{int}}^{eT} |\beta_i \cdot T_y\rangle\right|^2 \\ &+ \left|\langle e| H_{\mathrm{int}}^{eT} |\zeta_i \cdot T_z\rangle\right|^2 \\ =& |\alpha_i|^2 \cdot \gamma_x + |\beta_i|^2 \cdot \gamma_y + |\zeta_i|^2 \cdot \gamma_z\end{aligned} \tag{S12}$$

and

$$\begin{aligned}\Gamma'_i =& \left|\langle g| H_{\text{int}}^{Tg} |\varphi_i\rangle\right|^2 \\ =& \left|\langle g| H_{\text{int}}^{Tg} |\alpha_i \cdot T_x\rangle\right|^2 \\ &+ \left|\langle g| H_{\text{int}}^{Tg} |\beta_i \cdot T_y\rangle\right|^2 \\ &+ \left|\langle g| H_{\text{int}}^{Tg} |\zeta_i \cdot T_z\rangle\right|^2 \\ =& |\alpha_i|^2 \cdot \Gamma_x + |\beta_i|^2 \cdot \Gamma_y + |\zeta_i|^2 \cdot \Gamma_z \,.\end{aligned} \tag{S13}$$

Using these new transition rates, which inherit their magnetic field dependence from the states $|\varphi_i\rangle$, the steady state solution can be calculated for every magnetic field $\mathbf{B}$.

As the reference given by the NV center fixes only the z-orientation of TR12 triplet, the orientation of x- and y-axis still have to be obtained. This is achieved by rotating x- and y-axis around the z-orientation, always forming an orthogonal system. The resulting magnetic map is then graphically fitted to the real measurement via this rotational angle. With a clear match the y-orientation is found to lie in the plane formed by two sigma bonds also fixing x-orientation. The respective local frames for the remaining eleven orientations are obtained by the described rotations by 120° and by reorienting the z-orientation along another sigma bond ([111] in Diamond). Using these local frames leads to the twelve simulated magnetic maps in Fig. S3. For comparison, examples for all measured maps are listed in the same figure below.

From the fact that simulations and measurements match almost perfectly, it can be concluded that the proposed electronic structure (Fig. 1f) is indeed an accurate description for TR12. As the example of the magnetic map for a NV center (Fig S2b) shows, a different electronic structure would lead to a completely different magnetic map. This especially confirms the spin multiplicity of the metastable triplet.

VII. SIMULATING ODMR CONTRAST

As the measurement of magnetic fields is one of TR12's strong sides, it seems reasonable to dig further into the dependence of ODMR resonances on the magnetic field.

To simulate the ODMR contrast of TR12 centers, start from equation (S7) with updated transition coefficients $\gamma_i \to \gamma'_i$ and $\Gamma_i \to \Gamma'_i$ depending on the magnetic field $\mathbf{B}$ according to the previous section. The actual ODMR measurement can now be taken into account by adding additional transitions rates M between two of the triplet sub-levels $|\varphi_i\rangle$ and $|\varphi_j\rangle$ (equation (S14) for $\{i,j\} = \{1,2\}$). Driving this transition is achieved by applying a microwave with frequency ω fitting the energy difference between $|\varphi_i\rangle$ and $|\varphi_j\rangle$. The result is the same as in section IV. However, section IV was focused on the dynamics of the system while now the only goal is to calculate the resulting steady state and its excited state population respectively. Therefore the dynamics of Rabi oscillation in equation (S8) is replaced by a simple transition rate.

$$M = \begin{pmatrix} -P & \Gamma & \Gamma'_1 & \Gamma'_2 & \Gamma'_3 \\ P & -\Gamma - \gamma'_1 - \gamma'_2 - \gamma'_3 & 0 & 0 & 0 \\ 0 & \gamma'_1 & -\Gamma'_1 - M & M & 0 \\ 0 & \gamma'_2 & M & -\Gamma'_2 - M & 0 \\ 0 & \gamma'_3 & 0 & 0 & -\Gamma'_3 \end{pmatrix} \tag{S14}$$

As in section III, finding the eigenvector of this matrix to the eigenvalue $EW = 0$ (conservation of population) equals finding the steady state solution. The population of the excited state ρ_e proportional to the fluorescence intensity will now be a function of the microwave intensity (ρ_e=$\rho_e(M)$) which saturates for sufficiently large values of M. The ODMR contrast of TR12 centers η which we define as

$$\eta = \frac{\rho_e(M) - \rho_e(M=0)}{\rho_e(M=0)} \tag{S15}$$

clearly saturates along with $\rho_e(M)$. This value of saturation is referred to as ODMR contrast in the main text and supplementary.

In order to backwards calculate the magnetic field strength from ODMR measurements, the frequency of two transitions is required [7]. The effective ODMR contrast of a center for measuring magnetic fields is therefore given by its second strongest ODMR transition as displayed in Fig. 4 in the main text. The exact orientation of the magnetic field can not be derived from ODMR measurements on a single center, only a unique combination $\Delta = D\cos(2\theta) + 2E\cos(2\phi)\sin^2(\theta)$ [7]. However, by combining the information of differently oriented centers, it is a matter of pure trigonometry to receive the desired vector. Full vector magnetometry using TR12 centers, therefore requires 4 different ODMR frequencies belonging to two differently oriented centers. If one wants to give a measure, how good TR12 can be used for full vector magnetometry, it therefore seams reasonable to name the lowest contrast of these 4 ODMR frequencies. For a given magnetic field orientation one should therefor sim-

ulated the ODMR contrast of all three transitions for all twelve orientations of TR12. The contrast of each orientation is defined as the second highest ODMR contrast of all its transition. The ODMR contrast for Bulk measurements is then defined equal to the contrast of the orientation with second highest contrast. This procedure results in plots such as Fig. 5 a,b in the main text. For further illustration 2D plots are added in Fig. S4.

[1] Y. I. Khanin and O. A. Kocharovskaya, Inversionless amplification of ultrashort pulses and coherent population trapping in a three-level medium, J. Opt. Soc. Am. B **7**, 2016 (1990).

[2] E. Arimondo and G. Orriols, Nonabsorbing atomic coherences by coherent two-photon transitions in a three-level optical pumping, Letter.e al nuovo cimento **17** (1976).

[3] H. R. Gray, R. M. Whitley, and C. R. Stroud, Coherent trapping of atomic populations, Opt. Lett. **3**, 218 (1978).

[4] H.-I. Yoo and J. Eberly, Dynamical theory of an atom with two or three levels interacting with quantized cavity fields, Physics Reports **118**, 239 (1985).

[5] R. G. Brewer and E. L. Hahn, Coherent two-photon processes: Transient and steady-state cases, Phys. Rev. A **11**, 1641 (1975).

[6] R. M. Whitley and C. R. Stroud, Double optical resonance, Phys. Rev. A **14**, 1498 (1976).

[7] G. Balasubramanian et al., Nanoscale imaging magnetometry with diamond spins under ambient conditions, Nature **455**, 648 (2008).

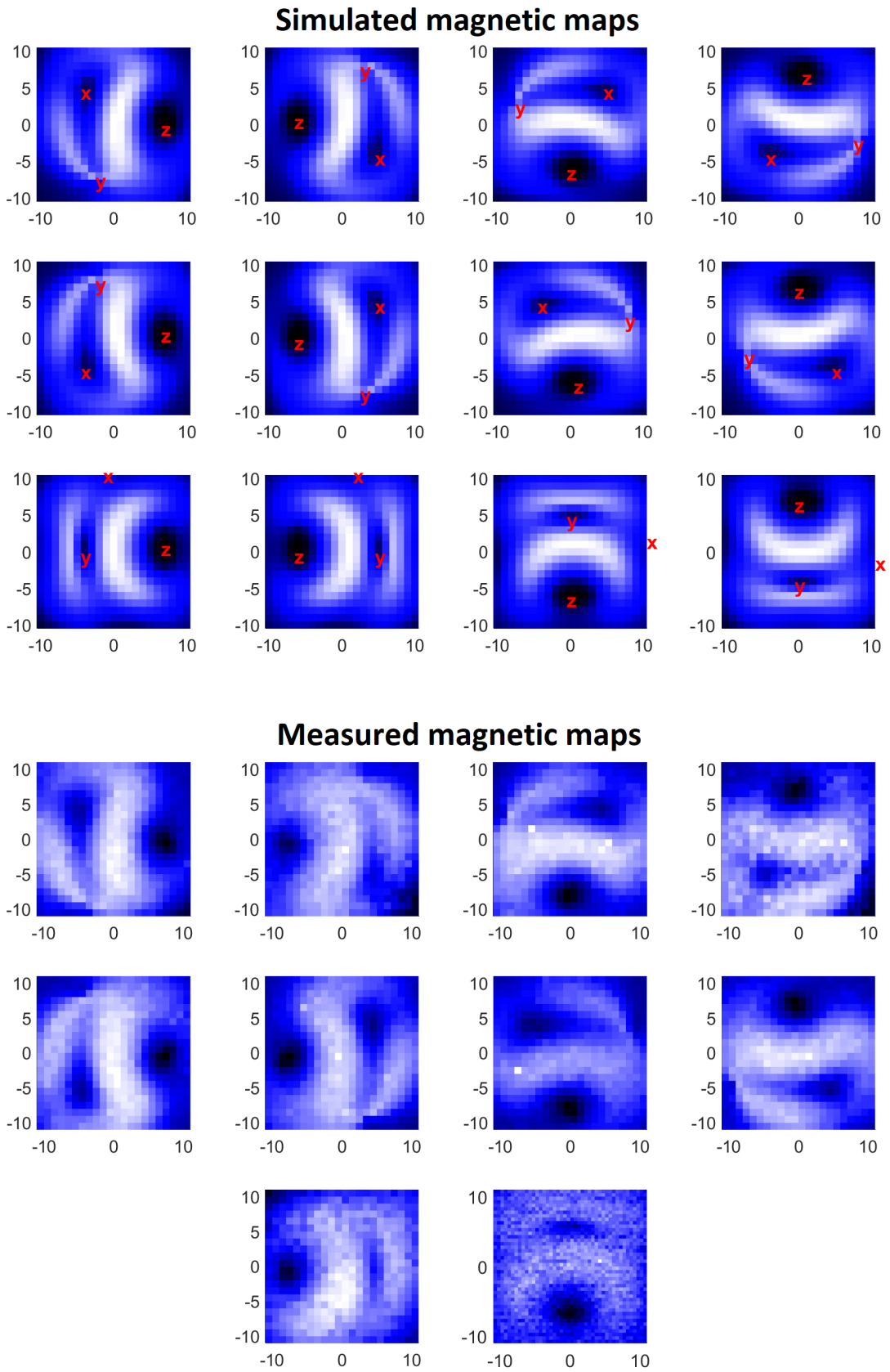

FIG. S3. Simulated (top) and measured (below) magnetic maps for TR12. The axes display the magnet position in millimeters while the brightness is displayed by coloring. The two missing maps have not been observed so far.

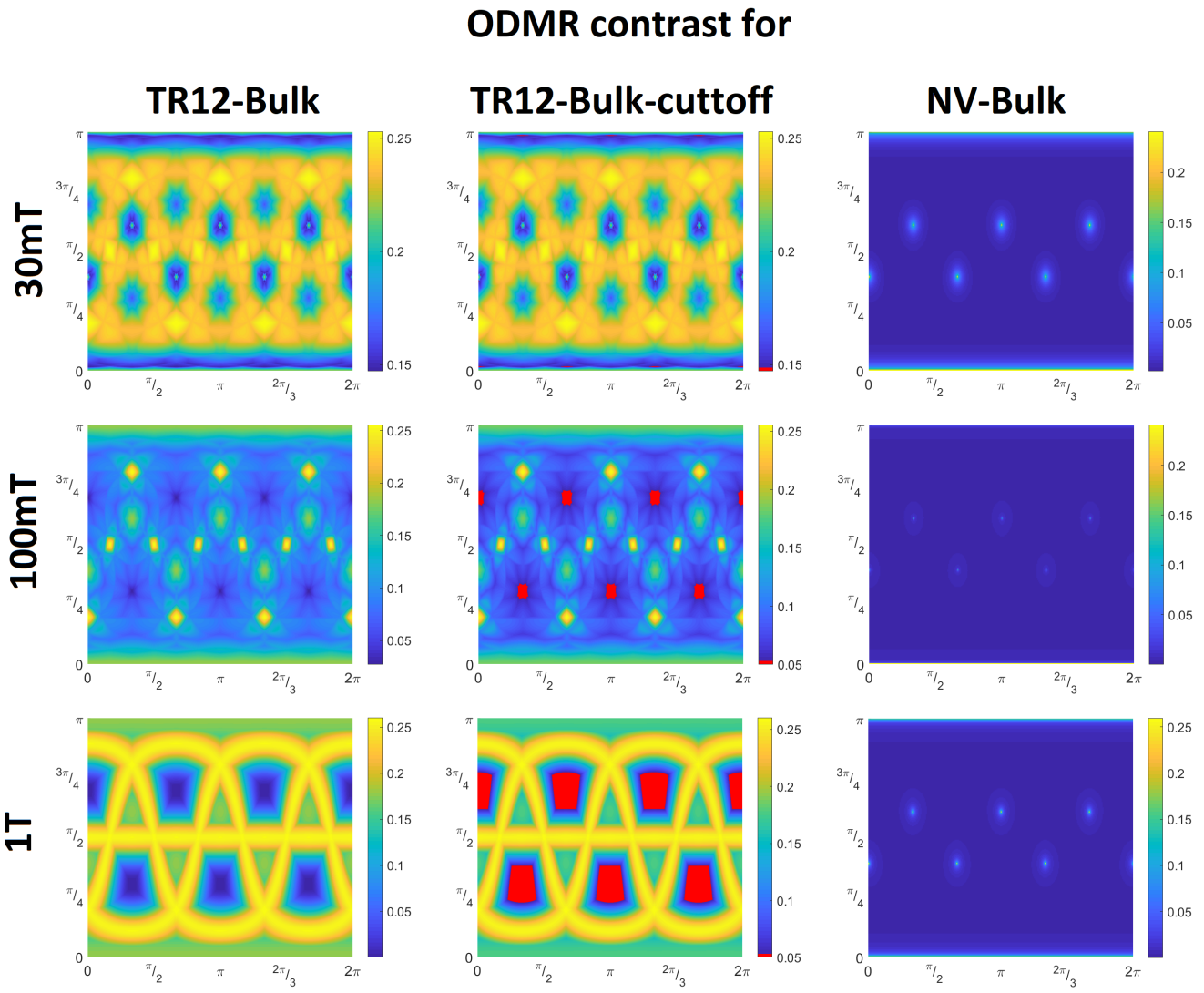

FIG. S4. ODMR contrast of TR12 Bulk samples with (column 2) and without (column 1) cut-off depending on magnetic field orientation ϕ (x-axis) and θ (y-axis). Column 3 show the bulk contrast for NV centers. For line 1 (30 mT) the cut-off was set at 15 %. For line 2 (100 mT) and line 3 (1 T) it was set to 5 %. For TR12 the ODMR contrast was calculated as described in section VII. For NV the picture displays simply the highest contrast of all NV orientations available.